Journal of the American Heart Association

ORIGINAL RESEARCH

Liver X Receptor Agonist AZ876 Induces Beneficial Endogenous Cardiac Lipid Reprogramming and Protects Against Isoproterenol-Induced Cardiac Damage

Daniel Ritter, RPh; Madeleine Goeritzer, PhD; Arne Thiele, cand. med; Annelie Blumrich, Dr.rer.nat.; Niklas Beyhoff, MD; Katja Luettges, RPh; Elia Smeir, Dr.rer.nat.; Juliane Kasch, PhD; Jana Grune, PhD; Oliver J. Müller, MD; Robert Klopfleisch, PhD; Carsten Jaeger, PhD; Anna Foryst-Ludwig, PhD; Ulrich Kintscher, MD

BACKGROUND: It is known that dietary intake of polyunsaturated fatty acids may improve cardiac function. However, relatively high daily doses are required to achieve sufficient cardiac concentrations of beneficial omega-3 fatty acids. The liver X receptor (LXR) is a nuclear hormone receptor and a crucial regulator of lipid homeostasis in mammals. LXR activation has been shown to endogenously reprogram cellular lipid profiles toward increased polyunsaturated fatty acids levels. Here we studied whether LXR lipid reprogramming occurs in cardiac tissue and exerts cardioprotective actions.

METHODS AND RESULTS: Male 129SV mice were treated with the LXR agonist AZ876 (20 μmol/kg per day) for 11 days. From day 6, the mice were injected with the nonselective β-agonist isoproterenol for 4 consecutive days to induce diastolic dysfunction and subendocardial fibrosis while maintaining systolic function. Treatment with isoproterenol led to a marked impairment of global longitudinal strain and the E/e' ratio of transmitral flow to mitral annular velocity, which were both significantly improved by the LXR agonist. Histological examination showed a significant reduction in isoproterenol-induced subendocardial fibrosis by AZ876. Analysis of the cardiac lipid composition by liquid chromatography-high resolution mass spectrometry revealed a significant increase in cardiac polyunsaturated fatty acids levels and a significant reduction in saturated fatty acids by AZ876.

CONCLUSIONS: The present study provides evidence that the LXR agonist AZ876 prevents subendocardial damage, improves global longitudinal strain and E/e' in a mouse model of isoproterenol-induced cardiac damage, accompanied by an upregulation of cardiac polyunsaturated fatty acids levels. Cardiac LXR activation and beneficial endogenous cardiac lipid reprogramming may provide a new therapeutic strategy in cardiac disease with diastolic dysfunction.

Key Words: diastolic dysfunction ■ heart failure ■ lipids ■ liver X receptor ■ nuclear receptor

Heart failure (HF) is a leading cause of morbidity and mortality worldwide.[1] As many as 1 in 5 people are expected to develop HF during their lifetime. Two major forms of HF exist, HF with reduced ejection fraction and HF with preserved ejection fraction. Whereas multiple pharmacological interventions for the treatment of HF with reduced ejection fraction have been established, effective approaches for HF with preserved ejection fraction are still being sought.[2]

Numerous neurohormonal mechanisms are activated to preserve cardiac function during HF, such as the sympathetic nervous system.[3] Two hormones that are essential for the sympathetic nervous system are the catecholamines epinephrine and norepinephrine.[3]

Correspondence to: Ulrich Kintscher, MD, Charité - Universitätsmedizin Berlin, Institute of Pharmacology, Hessische Str. 3–4, 10115 Berlin, Germany. E-mail: ulrich.kintscher@charite.de

Supplementary Material for this article is available at https://www.ahajournals.org/doi/suppl/10.1161/JAHA.120.019473

For Sources of Funding and Disclosures, see page 8.

JAHA is available at: www.ahajournals.org/journal/jaha

CLINICAL PERSPECTIVE

What Is New?

- Pharmacological liver X receptor activation protects against catecholamine-induced cardiac damage and diastolic dysfunction.
- Liver X receptor activation endogenously reprograms the cardiac lipid profile toward higher levels of cardioprotective polyunsaturated fatty acids.

What Are the Clinical Implications?

- New liver X receptor agonists may provide a future therapeutic approach for cardiac diseases with diastolic dysfunction such as heart failure with preserved ejection fraction.

Nonstandard Abbreviations and Acronyms

CTRL	control
GLS	global longitudinal strain
ISO	isoproterenol
LXR	liver X receptor

Under pathological conditions, as they occur during HF with reduced ejection fraction and HF with preserved ejection fraction, the chronic overstimulation by catecholamines becomes adverse, causing hypoxia, dysfunction in molecular signaling, and cardiac contractility, eventually leading to left-ventricular remodeling, cardiac fibrosis, and cell death.[3] Isoproterenol (ISO) is a synthetic sympathomimetic amine with structural similarities to epinephrine and binds almost exclusively to β-adrenergic receptors. Prolonged and excessive β-adrenoreceptor stimulation, for example by ISO, mimics the pathophysiological conditions of HF and induces serious myocardial damage.[3] In the present model, ISO induces subendocardial cell death and fibrosis accompanied by a preserved ejection fraction but impaired global longitudinal strain (GLS) and a pathological E/e' ratio of transmitral flow to mitral annular velocity.[4]

The liver X receptors (LXR) α and β are nuclear hormone receptors that belong to the superfamily of ligand-activated transcription factors.[5] Owing to their involvement in lipid and glucose metabolism, as well as cholesterol homeostasis and inflammation, they became therapeutic drug targets of interest in pathologies such as atherosclerosis and metabolic disease.[5]

In the present study, we show that systemic application of the dual partial LXR agonist AZ876 significantly reduces catecholamine-mediated cardiac damage and dysfunction in mice. In parallel, AZ876 endogenously reprograms the cardiac lipid profile toward higher levels of cardioprotective polyunsaturated fatty acids (PUFAs). Our findings suggest that LXR-mediated cardiac lipid reprogramming may provide a promising approach to reduce catecholamine-mediated cardiac damage and to improve diastolic dysfunction.

METHODS

The data that support the findings of this study are available from the corresponding author upon reasonable request. All animal procedures were performed according to the guidelines of the Charité - Universitaetsmedizin Berlin, Germany and were approved by the Landesamt für Gesundheit und Soziales (Berlin, Germany) for the use of laboratory animals and according to the current version of the German Law on the protection of animals.

Male 129SV mice (Janvier Labs, France) were kept in a temperature-controlled facility in individually ventilated cages. The amount of light was controlled to imitate a 12-hour day-night rhythm. Eight-week-old animals were randomized and divided into 4 groups (control[CTRL]-vehicle [VEH] n=10, CTRL-ISO n=10, AZ876-VEH n=12, and AZ876-ISO n=12). Mice either received a regular control diet (V1127-000, ssniff, Soest, Germany) (CTRL) or a diet supplemented with the LXR agonist AZ876 (AZ876) at 20 μmol/kg per day. After 6 days, mice either received a daily subcutaneous NaCl (VEH) or ISO injection over 4

Figure 1. LXR agonist AZ876 attenuates ISO-induced impairment in cardiac function.
A, Study design. Male 129SV mice were treated with either a control diet (CTRL) or a diet supplemented with the LXR agonist AZ876) and received one subcutaneous injection on 4 consecutive days, either with NaCl (VEH) or with isoproterenol (ISO). **B**, Left ventricular ejection fraction and (**C**) left ventricular cardiac output were assessed by echocardiography. **D**, Representative strain images in long-axis view (left) and short-axis view (right) asterisks identify papillary muscles. **E**, Global longitudinal strain (GLS), (**F**) Global circumferential strain (GCS), and (**G**) Global radial strain (GRS). **H**, E/e' ratio of transmitral flow to mitral annular velocity. **I**, Representative images of collagen content in cardiac cross-sections of the 4 treatment groups. Heart samples were fixated in paraffin and stained with Picrosirus red to visualize collagen content in red. **J**, Quantitative analysis of collagen content in the (sub-) endocardium (left) and epicardium (right). Data presented as mean ± SEM, n=10–12 per group, *=P<0.05, **=P<0.01 2-way ANOVA with Bonferroni post hoc test. Ao indicates aorta; LA, left atrium; and LV, left ventricle.

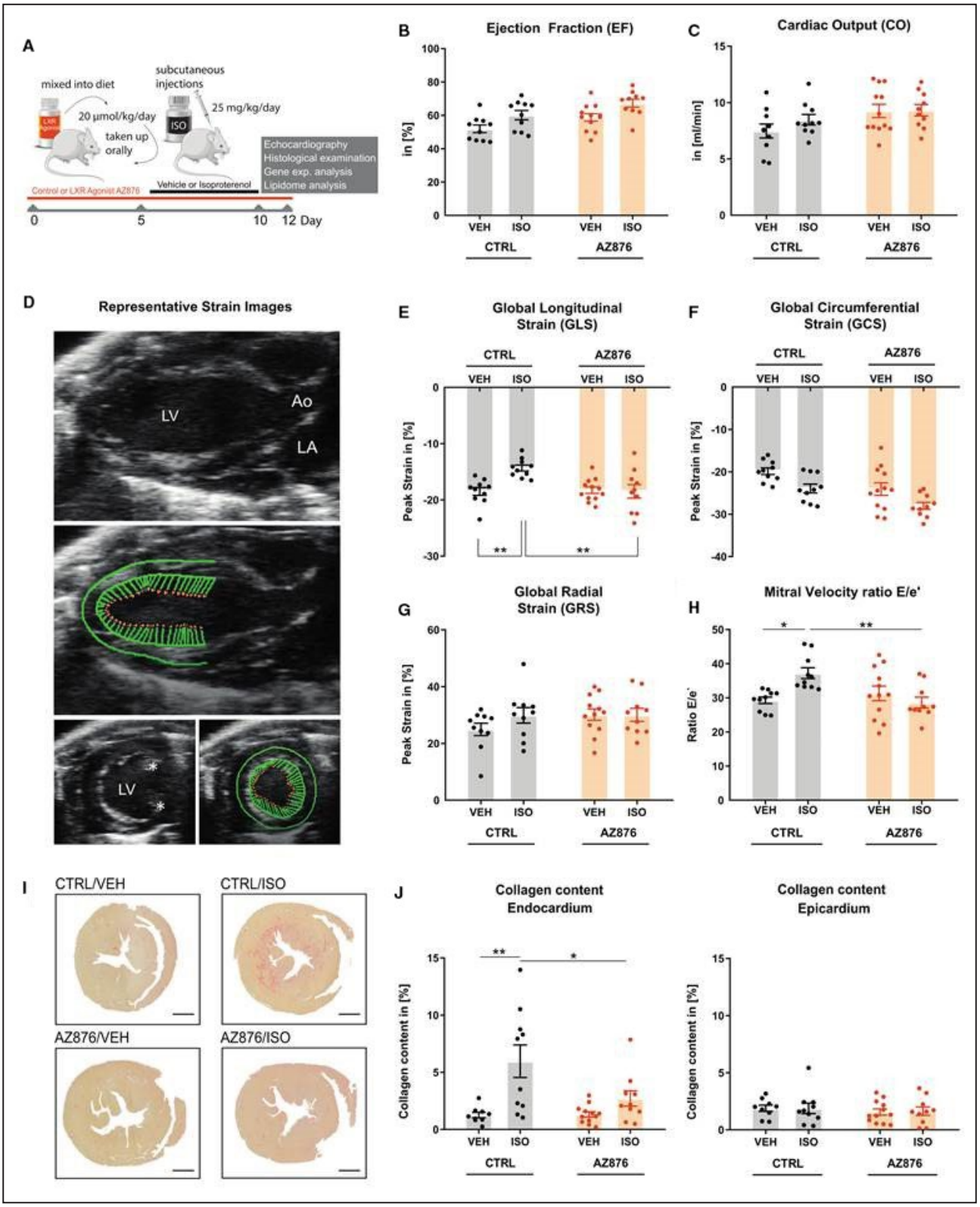

consecutive days. Two days after the last injection, the cardiac phenotype of the mice was characterized by both conventional and speckle tracking echocardiography. Post mortem analyses were performed in a blinded fashion. Additionally, histological analyses, quantitative reverse transcription-polymerase chain reaction-based analyses, and analytical analyses of lipid composition by liquid chromatography-high

resolution mass spectrometry were performed on heart tissue.

The cell experiments were performed with the murine cardiomyocyte cell line HL-1.[6] The cell line was initially provided by Prof. W.C. Claycomb (Louisiana State University, USA) and cultivated in Claycomb medium supplemented with 10% fetal bovine serum, 1% P/S, norepinephrine (0.1 mmol/L), and L-glutamine (2 mmol/L).

HL-1 cardiomyocytes were seeded in 6 well plates coated with fibronectin and gelatin. Starved cells were stimulated with the LXR agonist AZ876 for indicated time intervals and with indicated concentration.

Detailed methods are described in Data S1.

RESULTS

The LXR Agonist AZ876 Attenuates ISO-Induced Impairment in Cardiac Function

To investigate the cardiac effects of LXR activation in a mouse model of sympathetic activation and diastolic dysfunction,[4] the LXR agonist AZ876 was administered to male 129SV mice. Mice were treated with either a CTRL diet or a diet supplemented with the LXR agonist AZ876 for 6 days, followed by 4 consecutive subcutaneous injections of VEH (NaCl) or ISO to induce cardiac damage (Figure 1A).

Two days after the last ISO injection, heart function was assessed by conventional echocardiography and speckle tracking echocardiography. Systolic ejection fraction and cardiac output were found to be unchanged and were neither affected by the LXR agonist nor by ISO administration (Figure 1B and 1C). Specific analysis of myocardial deformation was performed by speckle tracking echocardiography (Figure 1D). It is known that the subcutaneous application of ISO at 25 mg/kg per day over 4 consecutive days leads to an impairment in the global longitudinal elongation.[5] However, the global radial strain, as well as the global circumferential strain, are not affected.[5] In this study, the application of ISO also led to a significant impairment in GLS, while the global radial strain and global circumferential strain remained unchanged (Figure 1E through 1G). More important, application of the LXR agonist significantly improved the GLS compared with the group treated with ISO alone (Figure 1E through 1G). In addition, significant differences were found in an essential parameter for diastolic function, the E/e' ratio of transmitral flow to mitral annular velocity (Figure 1H). The administration of ISO alone led to a significant increase of E/e', which was prevented by additional treatment with the LXR agonist (Figure 1H). Because the ratio between early mitral inflow velocity and mitral annular early diastolic velocity (E/e'), has become central in the guidelines for diastolic assessment, these data suggest that LXR activation may exert beneficial actions on diastolic function.

As previously shown, ISO-mediated impairment of GLS is associated with subendocardial fibrosis in the present model.[4] Accordingly, a significant increase of subendocardial fibrosis (red) was found in the CTRL/ISO-treated group as assessed by a Picrosirus red staining (Figure 1I and 1J). More important, the LXR agonist significantly reduced subendocardial fibrosis (Figure 1I and 1J). No fibrosis regulation was observed in the epicardium (Figure 1I and 1J).

Together these data show that pharmacological LXR activation reduces cardiac fibrosis and exerts beneficial actions on parameters of diastolic dysfunction.

The LXR Agonist AZ876 Mediates Cardiac Anti-Inflammatory Actions and Induces Enzymes Involved in the Synthesis of Omega-3 Fatty Acids

Ligand-activated LXR has been shown to exert potent anti-inflammatory actions.[5] To determine whether cardiac inflammation is altered by AZ876 in our model, we performed a quantitative polymerase chain reaction-based expression array of inflammatory response and autoimmunity genes in cardiac tissue samples from our mice (Figure 2A and 2B). ISO-treatment induced multiple proinflammatory genes including interleukins 1α, 6, and 18, chemokine (C-C motif) receptors 1 and 2, and

Figure 2. The LXR agonist AZ876 induces anti-inflammatory cardiac actions and LXR-target genes.
A and **B**, Reverse transcription quantitative polymerase chain reaction (PCR)-based cardiac gene expression analysis of inflammatory response and autoimmunity genes (locked nucleic acid-enhanced, SYBR® Green-based PCR array) (n=3/ group) (**A**) Partial least squares discriminant analysis (PLS-DA) of cardiac gene expression between the 4 groups, x-axis, principal component 1 (Comp1); y-axis, principal component 2 (Comp2), ellipses show 95% CI. **B**, Expression profiles of cardiac inflammatory and autoimmunity genes represented in a heatmap. Hierarchical clustering of normalized gene expression levels, shown as row z-scores. Clustering and heatmap were generated using MetaboAnalyst (**C**) Representative images of macrophage infiltration into cardiac tissue visualized by immunohistological staining for Mac-3, a macrophage surface glycoprotein. **D**, Relative gene expression of liver X receptor (LXR) target genes measured in apices of murine hearts. **E**, Relative gene expression of LXR target genes after 6h, 24h, and 48h of 10nM LXR agonist AZ876 stimulation, measured in HL-1 cells. Data presented as mean ± SEM, n=10–12 per group, *= $P<0.05$, **=$P<0.01$ 2-way ANOVA with Bonferroni post hoc test (**D**), or n=3; N=3, mean ± SEM, *=$P<0.05$, **=$P<0.01$, ***=$P<0.001$, 1-way ANOVA with Bonferroni post hoc test (**E**). AZ876 indicates LXR agonist AZ876; CTRL, control (dimethyl sulfoxide); ELOVL5, fatty acid elongase 5; FADS2, fatty acid desaturase 2; ISO, isoproterenol; SCD2, stearoyl-CoA desaturase 2; and VEH, vehicle (NaCl).

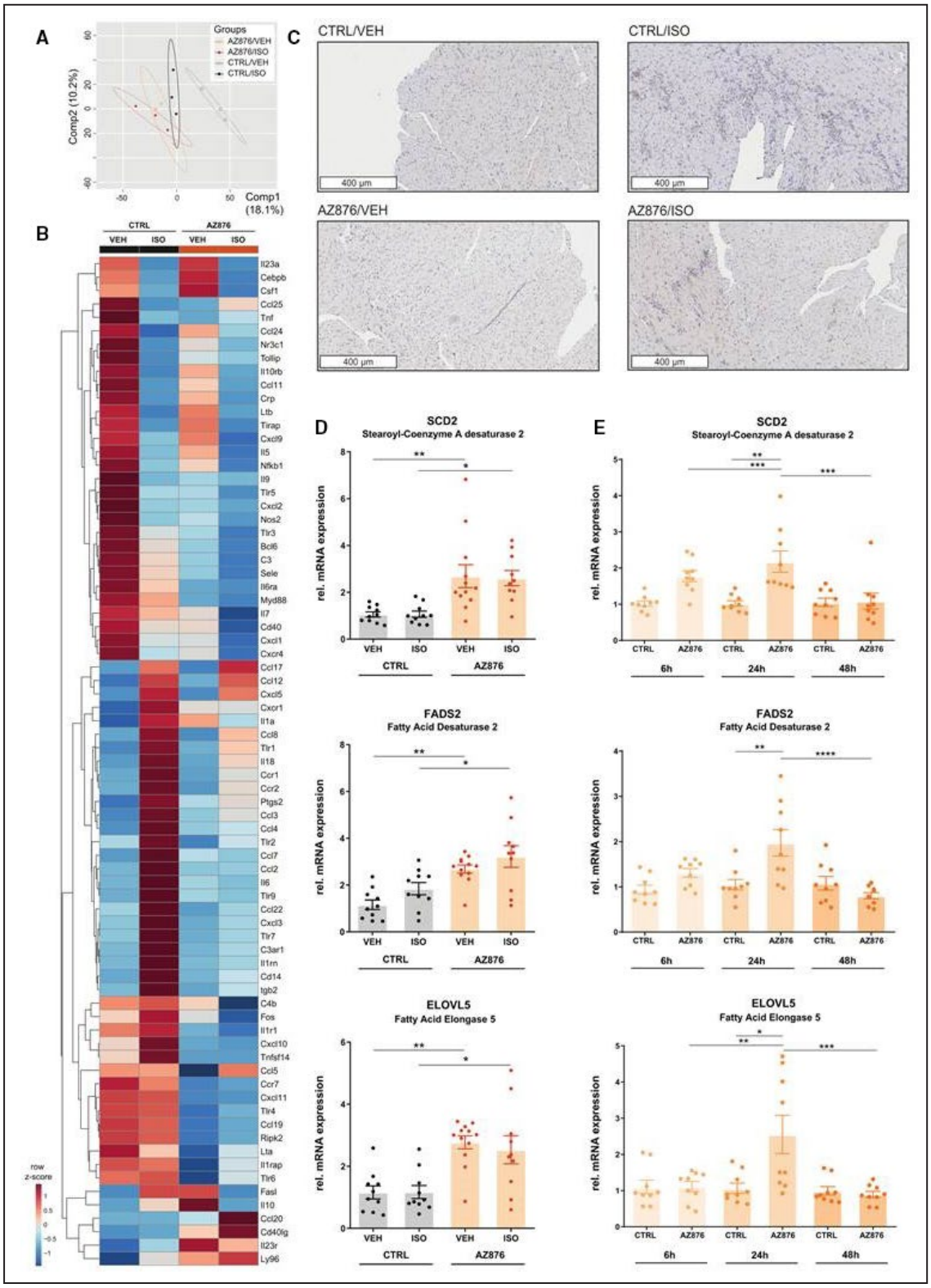

multiple chemokine (C-C motif) ligands, which were reduced by the LXR agonist (Figure 2B). In addition, immunohistological staining of cardiac cross sections for the macrophage marker Mac-3 revealed cardiac macrophage accumulation under ISO, which was attenuated with AZ876 (Figure 2C). Together, these data indicate an anti-inflammatory action of AZ876 in the hearts of our model.

To further prove cardiac LXR activation by AZ876 in our model, we next studied LXR target gene expression

in left ventricular (LV) samples. Administration of the LXR agonist resulted in a significant increase in the expression of LXR target genes involved in the synthesis of omega-3 fatty acids (FAs) compared with control (Figure 2D). Administration of ISO did not cause any significant changes in the expression of these genes compared with the control groups (Figure 2D). LXR-mediated cardiac regulation of genes involved in lipid metabolism was next studied in HL-1 cells. HL-1 cells were stimulated for different time intervals with AZ876 (10 nmol/L). Consistently with the data in LV samples, ligand-activated LXR resulted in a significant induction of stearoyl-CoA desaturase2, FA desaturase 2, and FA elongase 5 after 24 hours. (Figure 2E). Together these results demonstrate that AZ876 induces cardiac anti-inflammatory actions and LXR target gene expression involved in the process of lipid desaturation.

The LXR Agonist AZ876 Significantly Alters the Cardiac Lipid Profile Toward a Higher Content of Unsaturated FAs

Previously, LXR-mediated anti-inflammatory actions have been linked to its effects on lipid metabolism involving the synthesis of long chain PUFAs.[7] To clarify whether the anti-inflammatory actions of AZ876 are accompanied by beneficial actions on cardiac lipid composition, we next performed liquid chromatography-high resolution mass spectrometry-based lipidomics in LV samples from our mouse model.

Clustering of the treatment groups in a partial least squares discriminant analysis, shows that the groups treated with the LXR agonist (CTRL and ISO) differ markedly from the VEH-treated groups (CTRL and ISO) (Figure 3A). Looking more closely at how these differences occur, shows that 33 lipid species are significantly regulated (VEH versus LXR agonist) as presented in the heat map (Figure 3B).

Individual phosphatidylcholine and phosphatidylethanolamine lipid species consisting of monounsaturated FAs and PUFAs, especially the cardioprotective FA docosahexaenoic acid (FA 22:6 n-3), are found in a higher abundance in the groups treated with the LXR agonist (Figure 3C). To gain a deeper understanding of the degree of saturation of lipids species in the heart tissue, the abundances of the individual FAs were calculated (Figure 3D). The abundance of stearic acid (FA 18:0), the most abundant saturated FA, is reduced in the groups treated with the LXR agonist (Figure 3D). Among the monounsaturated FAs oleic acid (FA 18:1 n-9) had the highest abundance, and was reduced in heart tissue of mice treated with the LXR agonist (Figure 3D). Consistently with the induction of LXR-target genes involved in lipid desaturation, the highly abundant PUFA, docosahexaenoic acid, was significantly induced by the LXR agonist AZ876 (Figure 3D).

Taken together, these data show that pharmacological LXR activation induces overall cardiac lipid abundance by a predominant induction of lipid species containing cardioprotective PUFAs, which may be linked to the anti-inflammatory and cardioprotective actions of AZ876 in our model.

DISCUSSION

The present study demonstrates cardioprotective effects of the partial dual LXR agonist AZ876 in a murine model of ISO-induced cardiac damage. The assessment of cardiac function revealed a significant improvement in GLS and E/e' by AZ876 compared with ISO alone. The improvement in cardiac function was accompanied by reduced formation of subendocardial fibrosis. In parallel, AZ876 induced anti-inflammatory actions in the heart that may be linked to an LXR-mediated increase in the endogenous synthesis of cardiac PUFAs. This was supported by AZ876-mediated induction of cardiac FA elongases and desaturases

Figure 3. LXR agonist AZ876 significantly alters cardiac lipid composition toward a higher content in polyunsaturated fatty acids.

A, Partial least squares discriminant analysis (PLS-DA) of the cardiac lipid profile between the 4 groups, x-axis, principal component 1 (Comp1); y-axis, principal component 2 (Comp2), ellipses show 95% CI. **B**, Heatmap of 33 significantly regulated cardiac lipid species (VEH vs AZ876). Mice were treated with either CTRL or AZ876 supplementation and received 4 consecutive subcutaneous injections of either VEH or ISO. Clustering and heat map were created with MetaboAnalyst. Clustering of normalized intensities represented as z-scores, 2-way ANOVA, followed by Benjamini-Hochberg *P* value adjustment ($P<0.05$). **C**, Proposed beneficial lipid species containing monounsaturated FAs and the omega-3 fatty acid docosahexaenoic acid (FA 22:6 n-3, DHA). **D**, Log2-fold change of significantly altered FA moieties compared with CTRL_VEH. Values less than zero on the y-axis indicate lower fatty acid content, values greater than 1 indicate increase. The bubble size represents the measured intensity, which is analogous to the abundance of the FA. The intensities are normalized, and batch corrected. The FAs are sorted according to the degree of saturation. 2-way ANOVA followed by a Benjamini-Hochberg *P* value adjustment ($P<0.05$). Stearic acid, oleic acid, and docosahexaenoic acid are shown in magnification. Data presented as mean ± SEM, n=10–12 per group, *=$P<0.05$, ***=$P<0.01$, ****=$P<0.0001$, 1-way (**D**) or 2-way ANOVA (**C**) with Bonferroni post hoc test. AZ876 indicates LXR agonist AZ876; CTRL, control (diet); ELOVL5, fatty acid elongase 5; FA, fatty acid; FADS2, fatty acid desaturase 2; ISO, isoproterenol; LPC, lysophosphatidyl-choline; MUFA, monounsaturated fatty acids; LPG, lysophosphatidylglycerol; PC, phosphatidylcholine; PE, phosphatidylethanolamine; PUFA, polyunsaturated fatty acids; SCD2, stearoyl-CoA desaturase 2; SFA, saturated fatty acids; and VEH, vehicle (NaCl).

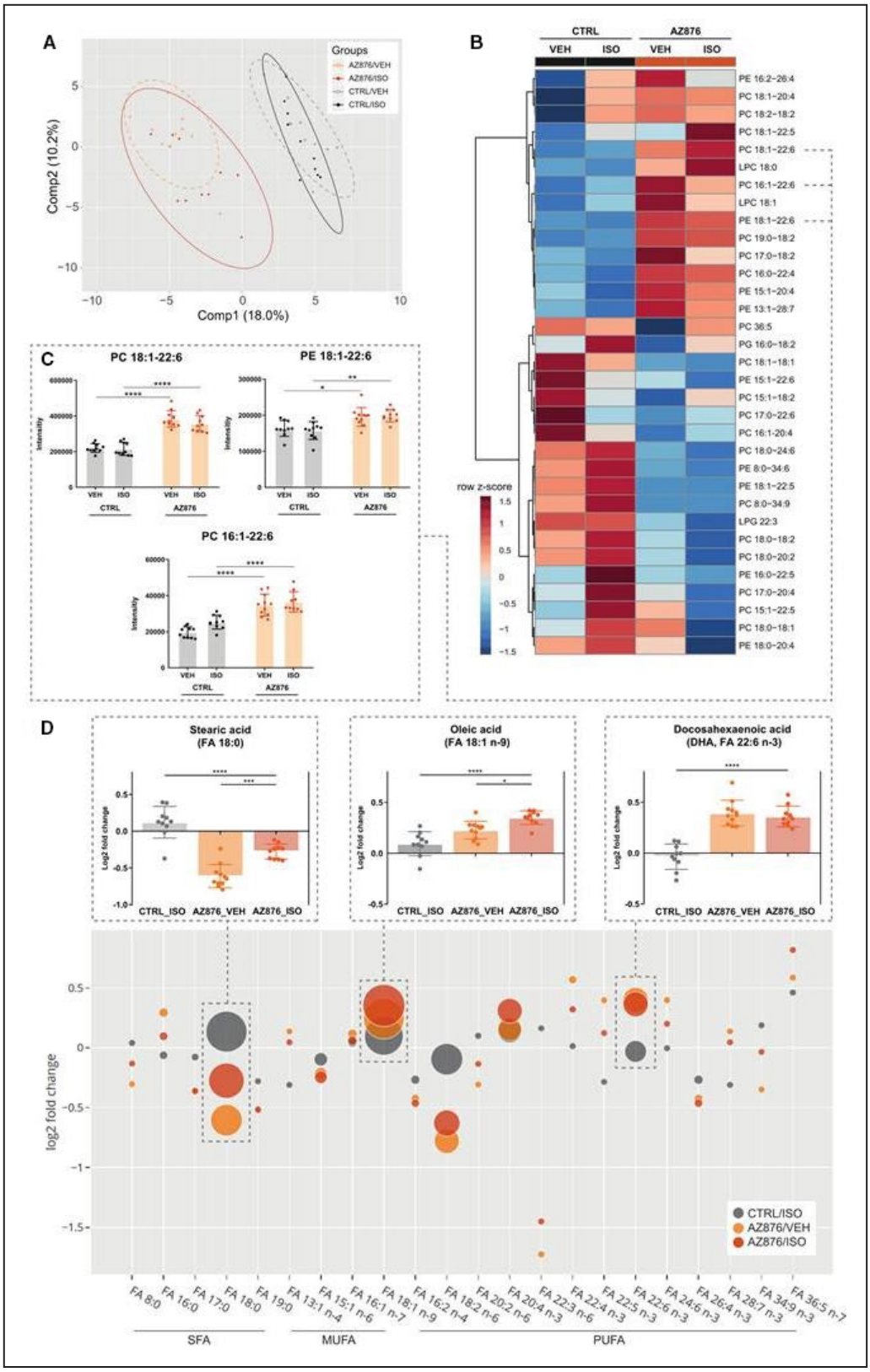

involved in the synthesis of PUFAs and by liquid chromatography-high resolution mass spectrometry-based cardiac lipid analysis, ultimately showing a significant decrease in saturated FAs and a significant increase of renowned PUFAs, such as docosahexaenoic acid.

Cardioprotective actions of pharmacological LXR activation have been described previously. Kuipers and

colleagues demonstrated that the full dual LXR agonist T0901317 prevented pressure-induced cardiac hypertrophy; however, this was associated with increased liver weight and hyperlipidemia in the T0901317-treated group.[8] In addition, Cannon and colleagues showed that AZ876 reduced LV hypertrophy improved systolic function and protected against cardiac fibrosis in a transverse aortic constriction model.[9] Importantly, AZ876 did not increase liver weight or plasma triglycerides.[9] These studies clearly demonstrated that pharmacological LXR activation is able to exert beneficial cardiac actions. However, the underlying biochemical and molecular mechanisms are still incompletely understood.[10]

Here we propose that ligand-activated LXR may exert cardiac antifibrotic actions through inhibition of an inflammatory response that might be linked to an increased LXR-mediated synthesis of cardiac anti-inflammatory PUFAs. It is well known that LXR mediates anti-inflammatory actions.[5] In parallel, LXR induces the endogenous synthesis of PUFAs.[7] Several studies have suggested a link between the cellular abundance of PUFAs and an inhibition of proinflammatory responses.[7,11,12] Rong and colleagues recently demonstrated that ligand-activated LXR drives the incorporation of PUFAs into cellular membrane phospholipids by the induction of LPCAT3 (lysophosphatidylcholine acyltransferase), an enzyme involved in phospholipid remodeling.[12] This process suppressed inflammation by inhibiting activation of the proinflammatory kinases c-Src (proto-oncogene tyrosine-protein kinase) and JNK (c-Jun N-terminal kinase) and by reducing the availability of proinflammatory mediators including arachidonic acid.[12] To finally prove that the elevated cardiac PUFA levels induced by AZ876 are indeed responsible for its anti-inflammatory and antifibrotic actions, additional experiments are required. In addition to our assumption, it is well known that LXR can directly affect antifibrotic and anti-inflammatory signaling by transcriptional mechanisms.[10] In particular, the repression of cardiac NF-kappaB (nuclear factor kappa-light-chain-enhancer of activated B cells) signaling by LXR plays an important role in this context.[13]

Antifibrotic actions and an improvement of diastolic dysfunction by PUFA administration have been recently also investigated in clinical studies. In a recent trial including 31 patients with ischemic HF, the administration of PUFAs (2 g/day for 8 weeks, 46% eicosapentaenoic acid and 38% docosahexaenoic acid) led to an improvement in GLS, a reduction in E/e' ratio, and reduced myocardial fibrosis, data consistent with our observations.[14] Antifibrotic actions of PUFAs have also been described in LV remodeling after acute myocardial infarction.[15]

In summary, this study demonstrates that pharmacological LXR activation results in a beneficial endogenous cardiac lipid reprogramming, involving the induction of cardiac PUFA levels. These LXR-mediated cardiac lipid changes are associated with anti-inflammatory and pronounced antifibrotic actions resulting in an improvement of diastolic function. Whether these data point toward a clinical beneficial action of LXR-ligands in heart diseases accompanied by fibrosis and diastolic dysfunction, such as HF with preserved ejection fraction, requires further investigation.

ARTICLE INFORMATION

Received September 22, 2020; accepted May 24, 2021.

Affiliations

Charité – Universitätsmedizin Berlin, corporate member of Freie Universität Berlin, Humboldt-Universität zu Berlin, Institute of Pharmacology, Center for Cardiovascular Research, Berlin, Germany (D.R., M.G., A.T., A.B., N.B., K.L., E.S., J.K., A.F., U.K.); DZHK (German Centre for Cardiovascular Research), partner site Berlin, Berlin, Germany (D.R., M.G., A.T., A.B., N.B., K.L., E.S., J.K., J.G., A.F., U.K.); Berlin Institute of Health, Berlin, Germany (N.B.); Charité –Universitätsmedizin Berlin, corporate member of Freie Universität Berlin, Humboldt-Universität zu Berlin, Institute of Physiology, Berlin, Germany (J.G.); Department of Internal Medicine III, University of Kiel, Germany (O.J.M.); DZHK (German Centre for Cardiovascular Research), partner site Hamburg/Kiel/Lübeck, Kiel, Germany (O.J.M.); Department of Veterinary Pathology, College of Veterinary Medicine, Freie Universität Berlin, Berlin, Germany (R.K.); and Federal Institute for Material Research and Testing, Berlin, Germany (C.J.).

Acknowledgments

The authors thank Beata Hoeft for her excellent technical assistance. Parts of this work will be used in the PhD thesis of DR. Open access funding enabled and organized by Projekt DEAL.

Sources of Funding

This work was supported by the DZHK (German Centre for Cardiovascular Research). DR is supported by a research grant of the Sonnenfeld Stiftung. NB is a participant in the BIH (Berlin Institute of Health) - Charité Junior Clinician Scientist Program funded by the Charité - Universitaetsmedizin Berlin and the Berlin Institute of Health. UK is supported by the DZHK; BER 5.4 PR, the Deutsche Forschungsgemeinschaft (DFG–KI 712/10-1), the Bundesministerium für Bildung und Forschung/Bundesinstitut für Risikobewertung (BMBF/ BfR1328-564m), and the Einstein Foundation/ Foundation Charité (EVF-BIH-2018–440).

Disclosures

None.

Supplementary Material

Data S1
References 16–22

REFERENCES

1. Benjamin EJ, Muntner P, Alonso A, Bittencourt MS, Callaway CW, Carson AP, Chamberlain AM, Chang AR, Cheng S, Das SR, et al.; American Heart Association Council on Epidemiology and Prevention Statistics Committee and Stroke Statistics Subcommittee. Heart disease and stroke statistics-2019 update: a report from the American Heart Association. *Circulation*. 2019;139:e56–e528. DOI: 10.1161/CIR.0000000000000659.
2. Ponikowski P, Voors AA, Anker SD, Bueno H, Cleland JGF, Coats AJS, Falk V, González-Juanatey JR, Harjola V-P, Jankowska EA, et al; and Authors/Task Force. 2016 ESC Guidelines for the diagnosis and treatment of acute and chronic heart failure: the Task Force for the diagnosis and treatment of acute and chronic heart failure of the

European Society of Cardiology (ESC) Developed with the special contribution of the Heart Failure Association (HFA) of the ESC. *Eur Heart J*. 2016;2016(37):2129–2200. DOI: 10.1093/eurheartj/ehw128.
3. Hartupee J, Mann DL. Neurohormonal activation in heart failure with reduced ejection fraction. *Nat Rev Cardiol*. 2017;14:30–38. DOI: 10.1038/nrcardio.2016.163.
4. Beyhoff N, Lohr D, Foryst-Ludwig A, Klopfleisch R, Brix S, Grune J, Thiele A, Erfinanda L, Tabuchi A, Kuebler WM, et al. Characterization of myocardial microstructure and function in an experimental model of isolated subendocardial damage. *Hypertension*. 2019;74:295–304. DOI: 10.1161/HYPERTENSIONAHA.119.12956.
5. Zelcer N, Tontonoz P. Liver X receptors as integrators of metabolic and inflammatory signaling. *J Clin Invest*. 2006;116:607–614. DOI: 10.1172/JCI27883.
6. Claycomb WC, Lanson NA Jr, Stallworth BS, Egeland DB, Delcarpio JB, Bahinski A, Izzo NJ Jr. HL-1 cells: a cardiac muscle cell line that contracts and retains phenotypic characteristics of the adult cardiomyocyte. *Proc Natl Acad Sci USA*. 1998;95:2979–2984. DOI: 10.1073/pnas.95.6.2979.
7. Li P, Spann N, Kaikkonen M, Lu M, Oh D, Fox J, Bandyopadhyay G, Talukdar S, Xu J, Lagakos W, et al. NCoR repression of LXRs restricts macrophage biosynthesis of insulin-sensitizing omega 3 fatty acids. *Cell*. 2013;155:200–214. DOI: 10.1016/j.cell.2013.08.054.
8. Kuipers I, Li J, Vreeswijk-Baudoin I, Koster J, van der Harst P, Sillje HH, Kuipers F, van Veldhuisen DJ, van Gilst WH, de Boer RA. Activation of liver X receptors with T0901317 attenuates cardiac hypertrophy in vivo. *Eur J Heart Fail*. 2010;12:1042–1050. DOI: 10.1093/eurjhf/hfq109.
9. Cannon MV, Yu H, Candido WM, Dokter MM, Lindstedt EL, Sillje HH, van Gilst WH, de Boer RA. The liver X receptor agonist AZ876 protects against pathological cardiac hypertrophy and fibrosis without lipogenic side effects. *Eur J Heart Fail*. 2015;17:273–282. DOI: 10.1002/ejhf.243.
10. Cannon MV, van Gilst WH, de Boer RA. Emerging role of liver X receptors in cardiac pathophysiology and heart failure. *Basic Res Cardiol*. 2016;111:3. DOI: 10.1007/s00395-015-0520-7.
11. Oishi Y, Spann NJ, Link VM, Muse ED, Strid T, Edillor C, Kolar MJ, Matsuzaka T, Hayakawa S, Tao J, et al. SREBP1 contributes to resolution of pro-inflammatory TLR4 signaling by reprogramming fatty acid metabolism. *Cell Metab*. 2017;25:412–427. DOI: 10.1016/j.cmet.2016.11.009.
12. Rong X, Albert C, Hong C, Duerr M, Chamberlain B, Tarling E, Ito A, Gao J, Wang BO, Edwards P, et al. LXRs regulate ER stress and inflammation through dynamic modulation of membrane phospholipid composition. *Cell Metab*. 2013;18:685–697. DOI: 10.1016/j.cmet.2013.10.002.
13. Wu S, Yin R, Ernest R, Li Y, Zhelyabovska O, Luo J, Yang Y, Yang Q. Liver X receptors are negative regulators of cardiac hypertrophy via suppressing NF-kappaB signalling. *Cardiovasc Res*. 2009;84:119–126. DOI: 10.1093/cvr/cvp180.
14. Oikonomou E, Vogiatzi G, Karlis D, Siasos G, Chrysohoou C, Zografos T, Lazaros G, Tsalamandris S, Mourouzis K, Georgiopoulos G, et al. Effects of omega-3 polyunsaturated fatty acids on fibrosis, endothelial function and myocardial performance, in ischemic heart failure patients. *Clin Nutr*. 2019;38:1188–1197. DOI: 10.1016/j.clnu.2018.04.017.
15. Heydari B, Abdullah S, Shah R, Francis SA, Feng JH, McConnell J, Harris W, Antman EM, Jerosch-Herold M, Kwong RY. Omega-3 fatty acids effect on post-myocardial infarction ST2 levels for heart failure and myocardial fibrosis. *J Am Coll Cardiol*. 2018;72:953–955. DOI: 10.1016/j.jacc.2018.06.018.
16. Leitman M, Lysyansky P, Sidenko S, Shir V, Peleg E, Binenbaum M, Kaluski E, Krakover R, Vered Z. Two-dimensional strain-a novel software for real-time quantitative echocardiographic assessment of myocardial function. *J Am Soc Echocardiogr*. 2004;17:1021–1029. DOI: 10.1016/j.echo.2004.06.019.
17. Reisner SA, Lysyansky P, Agmon Y, Mutlak D, Lessick J, Friedman Z. Global longitudinal strain: a novel index of left ventricular systolic function. *J Am Soc Echocardiogr*. 2004;17:630–633. DOI: 10.1016/j.echo.2004.02.011.
18. Tsugawa H, Cajka T, Kind T, Ma Y, Higgins B, Ikeda K, Kanazawa M, VanderGheynst J, Fiehn O, Arita M. MS-DIAL: data-independent MS/MS deconvolution for comprehensive metabolome analysis. *Nat Methods*. 2015;12:523–526. DOI: 10.1038/nmeth.3393.
19. Jaeger C, Lisec J. Statistical and multivariate analysis of MS-based plant metabolomics data. *Methods Mol Biol*. 2018;1778:285–296. DOI: 10.1007/978-1-4939-7819-9_20.
20. Ito K, Murphy D. Application of ggplot2 to Pharmacometric Graphics. *CPT Pharmacometrics Syst Pharmacol*. 2013;2.e79. DOI: 10.1038/psp.2013.56.
21. Chong J, Soufan O, Li C, Caraus I, Li S, Bourque G, Wishart DS, Xia J. MetaboAnalyst 4.0: towards more transparent and integrative metabolomics analysis. *Nucleic Acids Res*. 2018;46:W486–W494. DOI: 10.1093/nar/gky310.
22. Salatzki J, Foryst-Ludwig A, Bentele K, Blumrich A, Smeir E, Ban Z, Brix S, Grune J, Beyhoff N, Klopfleisch R, et al. Adipose tissue ATGL modifies the cardiac lipidome in pressure-overload-induced left ventricular failure. *PLoS Genet*. 2018;14.e1007171. DOI: 10.1371/journal.pgen.1007171.

Supplemental Material

Data S1.

Supplemental Methods

Cell culture

The cell experiments were performed with the myocardial cell line HL-1, which was derived from the AT-1 mouse atrial cardiomyocyte tumor line (6). The cell line was provided by Prof. W.C. Claycomb (†) (Louisiana State University, USA) and cultivated in Claycomb medium supplemented with 10 % FBS, 1 % P/S, norepinephrine (0.1 mM) and L-glutamine (2 mM).

The HL-1 cardiomyocytes were seeded in 6 well plates, which were previously coated with fibronectin and gelatin. At a confluence of 80 %, the HL-1 cardiomyocytes were starved with the described Claycomb medium, but only with a reduced FBS content of 0.5 % overnight. Cells were stimulated with10nM of the LXR-agonist AZ876 for 24h. The cells were then harvested and stored at -80°C for further analysis.

Diet preparation and pair feeding

A dry feed for mice (V1127-000) was purchased from (ssniff, Spezialdiäten GmbH). 900g of the feed was mixed with the LXR-agonist AZ876 until complete homogeneity was achieved. 1500g of water was added to the powder in portions, while the mass was mixed continuously. The moist and homogeneous mass was applied to blotting paper about 1 cm thick and cut into squares of 2 x 2 cm. After 48 hours drying, the solid squares were stored at -20°C. To keep the differences in food intake as small as possible, mice were kept in pairs in each cage. Previous

experiments in our group resulted in a food intake of 3.5g per mouse per day. Therefore, we provided 7g food per day, either with or without LXR agonist for each cage.

Echocardiography

Echocardiography was performed with an 18-38 MHz linear array transducer using a digital ultrasound system (Vevo 2100 Imaging System, VisualSonics, Toronto, Canada). Sample size was determined based on previous experience with this model (4). The mice were placed in a supine position on a movable, heated platform at 37°C. The mice were anesthetized with 1.5% isoflurane and their pleura was removed. At each echocardiographic examination, long- and short-axis B-mode parasternal views were recorded and conventional echocardiographic parameters were determined. Trans mitral flow measurements of ventricular filling velocity were obtained from the apical four-chamber view using the pulse wave Doppler to assess diastolic function. In addition, tissue Doppler images were obtained from this view at the septal fixation of the mitral valve. Using speckle tracking based strain analysis of two-dimensional echocardiographic images obtained from the parasternal long- and short-axis views, strain parameters in the longitudinal, radial and circumferential axis were quantified (16, 17). Longitudinal strain and radial strain were obtained from the longitudinal axis parasternal views, while circumferential strain in the short axis parasternal views was determined at the medial optic disc plane. All images were acquired at a frame rate of approximately 300 frames per second.

The longitudinal contraction and global longitudinal strain (GLS) represent the movement from the base to the apex. The global radial strain (GRS) represents

the myocardial thickening and thinning as the radial contraction in the short axis moves vertically to the long axis and the epicardium. Global circumferential strain (GCS) represents the radius movements in the short axis. To measure diastolic function, the mice were placed in an angled position with the head pointing slightly downward. In this position the apical four-chamber view is visual and the pulse wave doppler and tissue doppler can be determined. To determine the optimal position of the pulse wave doppler, the measurement point was placed slightly above the mitral valve with a strong color mode signal as an additional orientation aid. The incoming signals of the mitral valve show the individual phases and their contribution to filling. Since the mitral inflow represents the pressure differences between the ventricle and the atrium, all changes and anomalies in diastolic pressure affect the intensity and shape of the individual signals.

Image analyses

All image analyses were performed by one investigator and confirmed by a blinded second investigator using the software Vevo Lab (Fujifilm VisualSonics). The high-resolution images are displayed in slow motion, which allows an accurate analysis of the images despite a heart rate of about 450bpm. Official formulas of the American Society of Echocardiography were used to calculate all echocardiographic parameters. B-mode images of the parasternal longitudinal axis were used to semi-automatically analyze systolic function. Strain-based analyses were performed on B-mode images during three consecutive and electrocardiographically controlled cardiac cycles. Semi-automated tracking of the endocardium and epicardium was performed, with minor manual correction if necessary. GLS and GRS were evaluated using long-axis parasternal images

(227±1 frames/sec.). The myocardial tracings were placed starting from the middle basal region. GCS was assessed using images acquired in the short axis view (277±8 frames/sec.). The papillary muscles were used to standardize the image acquisition, but were excluded from the images. To determine the strain parameters, 48 points are placed virtually along the endocardial border and tracked over time to calculate the deformation over the cardiac cycle.

Lipid profiling and agonist detection in cardiac tissue

Lipid extraction and measurement were performed in cooperation with Dr. Carsten Jaeger (Federal Institute for Materials Research and Testing, Berlin, Germany). Dried tissue extracts were reconstituted in 100 µL isopropanol/acetonitrile/water (2:1:1). 5 µL aliquots were injected into an Agilent 1290 UHPLC system (Agilent) coupled to a TripleTOF 6600 mass spectrometer (Sciex). Chromatographic separation was achieved by gradient elution (%A: 0 min, 60%; 1.2 min, 57%; 1.26 min, 50%; 7.2 min, 46%; 7.26 min, 30%; 10.8 min, 0%; 12.96 min, 0%; 13.02 min, 60%; 14. 4 min, 60%) using a solvent system of 60:40 v/v acetonitrile/water (A) and 90:10 v/v isopropanol:water (B), both containing 10mM ammonium formate and 0.1% formic acid. The column used was a 2.1 mm × 75 mm × 1.7 µm CSH-C18 UPLC column (Waters) equipped with a 0.2 µm inline filter. The flow rate was 0.5 mL/min and the column temperature 55 °C. Electrospray ionization was performed in negative mode (ESI-) with the following settings: Alternating MS and MS/MS scans were recorded using sequential window-based acquisition of all theoretical fragment ion mass spectra (SWATH) (m/z 400-1250, window width 25 Da). Mass calibration was performed at the beginning of the sequence using an ESI (-) tune

mix (Sciex). For data analysis, MS files were converted into the ABF format (Analysis Base File) and imported into MS-DIAL (18). A lipidomics project was created ("Soft Ionization", "Data independent MS/MS", "Profile data", "Negative ion mode", "Lipidomics") and parameter settings were adjusted to match chromatographic and MS settings. After completion of data processing, results were exported to a text file and further analyzed with a user defined R script. In particular, data were filtered for sparse metabolites and contradictory peak allocations were resolved. Finally, peak intensities were normalized and corrected for batch effects as described (19).

Data processing

The PLS-DA were calculated with R package ”caret”. Scores and loadings diagrams were generated with R package ggplot2 (20).

The Heatmaps were created with the online tool MetaboAnalyst (21). Thirty-three out of 117 detected lipid species were significantly altered by LXR treatment. The *p*-values obtained by two-way ANOVA were adjusted using the Benjamini-Hochberg correction ($p<0.05$). The clustering in the lipid Heatmap was generated using average clustering and auto scaling, and shown are the color-coded intensities. Similarly, the Heatmap showing gene expression profiles of cardiac inflammatory & autoimmunity genes was generated. Average clustering and auto scaling was applied, and shown are the color-coded gene expression levels.

Histological analyses

The histological preparations and analyses were carried out in cooperation with Robert Klopfleisch from the Department of Veterinary Pathology, Free University

Berlin, Germany. At the end of the study organs of the mice were collected. The hearts were cut using a mouse heart matrix with a 0.5 mm incision. The apex, a mid-ventricular ring and the upper part of the heart were cut through and immediately formalin-fixed. The fixed midventricular ring was embedded in paraffin and the incisions were transferred to slides. The histological slides were stained with Picrosirus red to determine the collagen content. Endocardium and epicardium were defined manually using the Aperio ImageScope software. The collagen content was then automatically calculated as the percentage of collagen fibers stained with Picrosirus Red over the entire image area. To visualize the degree of macrophage infiltration, histological slides were stained for the Mac-3 marker, a macrophage surface glycoprotein, using an anti-mouse Mac3 antibody in a dilution 1:500 (#550292, BD Bioscience, CA, USA).

RNA extraction from HL-1 cells

The RNA expression was carried out with the Machery-Nagel NucleoSpin ®RNA kit. The cells were lysed in a mixture of RA1 lysis buffer and one percent β mercaptoethanol. β-Mercaptoethanol is a reducing agent that irreversibly denatures RNases by reducing disulfide bonds and destroying the native conformation required for enzyme functionality. 35 µL of 70 % ethanol were added and the sample was resuspended. The entire sample was transferred to a NucleoSpin ®RNA column and centrifuged (30 sec at 11 000 rpm). 350 µl membrane desalination buffer (MDB) was added. Salt removal significantly increases the effectiveness of rDNase digestion. After centrifugation (1 minute at 11 000 rpm) 95 µl rDNAse and reaction buffer were added to the column. After 15 minutes incubation at room temperature, 200 µl wash buffer RAW2 were

added to inactivate rDNAse. A second and third washing step was performed by adding 600 µl or 250 µl Wash Buffer RAW3. As a final step, 40 µl RNAse-free water was added to the column and centrifuged at 11 000 rpm for 1 minute. The RNA concentration was measured immediately with a spectrophotometer (NanoDrop). The RNA samples were stored at -80°C.

RNA extraction from cardiac tissue

Tissue samples from the heart tips were frozen in liquid nitrogen. The samples were mechanically comminuted and homogenized to obtain a fine tissue powder. 5 to 10 milligrams of the sample were weighed and collected. All steps were carried out with tools and containers that were cooled in liquid nitrogen to prevent thawing of the material and thus prevent RNA degradation. The RNA was isolated with the RNeasy® Micro Kit. The samples were placed in lysis tubes containing ten ceramic beads (lysis beads) to macerate the tissue and a mixture of RLT lysis buffer and 1% β mercaptoethanol. The lysis tubes were placed in a SpeedMill for 30 seconds at 13,000 rpm and immediately placed on ice. 295 µl RNAse-free water and 5 µl Proteinase K were added to the lysate and incubated for 10 min at 55°C. The samples were centrifuged for 3 minutes at 10,000 rpm. 225 µl absolute ethanol were added and the whole sample was transferred to an RNeasy-MinElute-Spin column. After 15 seconds centrifugation at 10 00 rpm 350 µl wash buffer RAW1 was added. 80 µl of a mixture of DNAse and RDD buffer were added and the samples incubated at room temperature. Buffer RDD ensures efficient on-column digestion of the DNA and also ensures that the RNA remains bound to the column. After 15 minutes 350 µl RW1 buffer was added, followed by 500 µl RPE buffer and 500 µl 80% ethanol. After 2 minutes

centrifugation at 11 000 rpm and 5 minutes centrifugation at full speed, 15 µl RNAse-free water was added and incubated at room temperature for 2 minutes. After a final centrifugation step for 1 minute at 11 000 rpm, the RNA concentration was measured with a spectrophotometer (NanoDrop). The RNA samples were stored at -80°C.

Single qRT-PCR analyses and qRT-PCR inflammation and autoimmunity assay

As previously described (22), RNA was reverse transcribed with reverse transcriptase, RNAsin and dNTPs (Promega) according to the manufacturer's protocol. The mRNA analysis was performed by quantitative RT-PCR analysis in presence of the fluorescent dye SYBR-Green (Life Sciences). The qRT-PCR results were normalized to 18S. Primer sequences are as follows:

Gene	*Forward Primer 5´-3´*	*Reverse Primer 3´-5´*
18S	CCTGAGAAACGGCTACCACAT	TTCCAATTACAGGGCCTCGA
Elovl5	ATGGAACATTTCGATGCGTCA	GTCCCAGCCATACAATGAGTAAG
FADS2	AAGGGAGGTAACCAGGGAGAG	CCGCTGGACCATTTGGTAA
SCD2	GCATTTGGGAGCCTTGTACG	AGCCGTGCCTTGTATGTTCTG

mRNA expression analyses of genes involved in inflammatory response and autoimmunity were performed using the QuantiNova LNA qPCR Assay (#249950 SBMM-077ZA, Qiagen, Hilden, Germany). Assays were performed according to the manufacturer's protocol.

Statistical methods

Data are presented as mean ± SEM. Statistical analyses were performed using GraphPad Prism 8 (GraphPad Software, United States). For comparison of more than two groups, two-way analysis of variance (ANOVA) followed by Bonferroni post-hoc test was used. A value of $p < 0.05$ was considered statically significant. Following levels of statistical significance were used: * $p < 0.05$, ** $p < 0.01$, *** $p < 0.001$, **** $p < 0.0001$. The determination of the group size for *in vivo* experiments was based on our experience with the ISO model (4). For analysis of lipidome data p-values were adjusted by Benjamini-Hochberg correction to avoid alpha inflation. Statistical significance was assumed at FDR-adjusted p-values of $p < 0.05$. Lipids were normalized to total lipid abundance in samples and either log2-transformed or presented in measured intensities. For visualization, the log2fold changes of the CTRL_VEH group were averaged over all samples and log2 fold changes were calculated for the remaining groups compared to the control group.